Influence of Bi on embedded nanocrystal formation and thermoelectric properties of GaAs

M. V. Warren,[1] J. C. Canniff,[1] H. Chi,[2] F. Naab,[3] V. A. Stoica,[2] R. Clarke,[2] C. Uher,[2] and R. S. Goldman[1,2]
[1]*Department of Materials Science and Engineering, University of Michigan, Ann Arbor, Michigan 48109, USA*
[2]*Department of Physics, University of Michigan, Ann Arbor, Michigan 48109, USA*
[3]*Department of Nuclear Engineering and Radiological Sciences, University of Michigan, Ann Arbor, Michigan 48109, USA*

(Received 31 December 2014; accepted 19 January 2015; published online 10 February 2015)

We have examined the influence of Bi on embedded nanocomposite formation and the resulting thermoelectric properties of GaAs. Bi implantation amorphizes the GaAs matrix, reducing both the free carrier concentration (n) and the electrical conductivity (σ). Following rapid thermal annealing, the matrix is transformed to single crystal GaAs with embedded Bi nanocrystals (NCs). In comparison to a GaAs reference, the Bi NC-containing films exhibit a sizeable reduction in thermal conductivity (κ), leading to a 30% increase in the thermoelectric figure-of-merit. We also present a universal trend for the influence of microstructure on the n-dependence of σ and κ. © *2015 AIP Publishing LLC*. [http://dx.doi.org/10.1063/1.4906992]

I. INTRODUCTION

Nanocomposite materials have been identified as promising candidates for high figure-of-merit thermoelectric materials. Due to the increased control of the density of states and hence, the energies of charge carriers, nanocomposite materials are predicted to have significantly higher thermoelectric figures-of-merit ($Z = S^2\sigma/\kappa$, where S is the Seebeck coefficient, σ is the electrical conductivity, and κ is the thermal conductivity) than their bulk counterparts.[1] For example, enhancements of Z due to low dimensionality have been reported for Bi_2Te_3/Sb_2Te_3 superlattices relative to those of bulk $Bi_{2-x}Sb_xTe_3$,[2] and for embedded Si nanocrystals (NCs) in SiGe relative to those of bulk SiGe.[3] Furthermore, enhancements of S for p-type Sb_2Te_3 with nanoscale Pt inclusions relative to those of bulk Sb_2Te_3 have been reported.[4] Finally, reductions in κ with respect to bulk Si have been predicted for Si-Ge nanocomposites consisting of low-κ Ge nanowires in a higher-κ Si matrix.[5] Interestingly, a grain-size dependent κ has been reported for $CoSb_3$[6] and explained by a model, in which phonon scattering increases with increasing grain boundary density.[7] However, the grain boundaries which scatter phonons are also expected to scatter electrons, reducing the electrical conductivity. For example, we recently reported a ~50% decrease in GaAs κ for GaAs with nanometer-sized grains and embedded In NCs (poly-GaAs:In).[8] However, the reduction in κ occurred simultaneously with a ~80% reduction in σ, yielding an overall reduction in Z.[8] To decrease κ, while minimizing the impact on σ, a strategy for the formation of embedded nanocomposites consisting of embedded metallic NCs in a single-crystal matrix is needed. Here, we examine the influence of Bi on the ion-beam synthesis and thermoelectric properties of GaAs. Due to the low solubility of Bi in GaAs,[9] Bi NCs are expected to readily nucleate in GaAs. Although low dose Bi^+ implantation at high (low) energies has been used to produce damage tracks in GaAs:Bi[10] (electronic states in GaP and GaAs[11,12]), ion-beam synthesis of embedded Bi NCs in GaAs has not been explored.

Here, we examine the effects of Bi^+ fluence on the microstructure and thermoelectric properties of the GaAs:Bi films. For the as-implanted films, the microstructure consists of a-GaAs, with or without crystalline remnants, voids, and/or ripples. Following rapid-thermal annealing (RTA), all films have transformed to single crystal GaAs with embedded Bi NCs, presumably due to Bi enhanced diffusion and segregation. For the Bi NC-containing films, κ is reduced to 30 to 50% of that of the GaAs reference, presumably due to phonon scattering at Bi NC/GaAs interfaces. Considering the reductions in σ and n, the NC-containing films exhibit a ~30% increase in the room temperature figure-of-merit, Z. We discuss the role of microstructure on the electrical and thermal conductivity of the GaAs:Bi films through a comparison with those of poly-GaAs:In and GaAs:N films.

This article is organized as follows. In Sec. II, we describe the methods for synthesizing and characterizing the GaAs:Bi films, including ion implantation, electrical conductivity, Hall effect, Seebeck coefficient, and time-domain thermoreflectance (TDTR) measurements. Investigations of the microstructure of the films and the influence of the microstructure on the thermoelectric properties are presented in Sec. III. A summary is presented in Sec. IV.

II. EXPERIMENTAL PROCEDURES

For these investigations, GaAs films were grown on semi-insulating (001) GaAs substrates using Ga, Al, As_2, and Si, as described elsewhere.[13] All samples consisted of an undoped GaAs buffer (250 nm thick), followed by Si-doped layers of GaAs (500 nm thick) and an AlAs sputter-mask (50 nm thick), all grown at 580 °C. The target free carrier concentration was 1×10^{18} cm^{-3}, within 50% of that predicted to maximize the GaAs power factor.[14] Following growth, a portion of the film was reserved as a reference sample, while the remainder was

implanted with 100 keV Bi^+, at fluences of 1.4×10^{16}, 2.8×10^{16}, and 5.6×10^{16} cm^{-2}, referred to as "low," "medium," and "high" fluence films. For the low and medium (high) fluence films, the AlAs layer is expected to be partially (fully) sputtered away.[15] To minimize channeling effects during implantation, a 7° angle of incidence with respect to the sample surface normal was utilized. During implantation, the substrate temperature was maintained at 77 K. Following implantation, RTA was performed in argon gas for 30 s at 450 °C. During RTA, a GaAs proximity cap was used to minimize As out-diffusion.

Following growth and/or implantation and/or RTA, the temperature-dependence of the Seebeck coefficient, $S(T)$, room temperature Hall effect, and electrical conductivity (σ) of the films were measured, as described in Ref. 8. We note here that the GaAs:Bi films consist primarily of single-crystal GaAs, a cubic lattice, which is isotropic and contains randomly distributed rhombohedral Bi NCs. As a consequence, the measured thermoelectric properties are also assumed to be isotropic, such that in-plane and cross-plane thermal conductivities are assumed to be equivalent, similar to the analysis of ErAs/InGaAs nanocomposites.[16] Our experiments relied upon optical TDTR measurements[17] using films prepared with and without an evaporated Al transducer layer. In this approach, pump-probe experiments are performed using short (~100 fs) pump pulses from an Er-doped fiber laser (1550 nm), followed by probe pulses from a frequency-doubled Er-doped fiber laser operating at 150 fs (780 nm). Finally, the reflection of the probe beam from the surface is measured using a balanced amplified Si photodetector with 1 MHz bandwidth (Thorlabs, PDB 120 A). During the pump-probe experiments, the pump pulse deposits energy at the surface; during the subsequent decay of the surface temperature, the corresponding decay in the amplitude of the probe pulse is monitored via the time-dependence of the measured surface reflectivity. Finally, an analysis of the thermoreflectance temporal decay, which is associated with heat flow away from the film, is used to extract the film thermal conductivity, as described in the Appendix. To examine the microstructure of the films, cross-sectional transmission electron microscopy (TEM), Energy Dispersive X-Ray Spectroscopy (EDX), and high-angle annular dark field (HAADF) scanning transmission electron microscopy (STEM) were performed, as described in Ref. 8.

III. RESULTS

A. Microstructural evolution

Figure 1 presents typical bright-field TEM images of as-implanted (a) low, (c) medium, and (e) high fluence films, with corresponding selected-area diffraction (SAD) patterns as insets. For all three fluences, a ~90 nm amorphous surface layer is observed on top of single-crystal GaAs. The presence of the a-GaAs layer is confirmed by the diffuse halo in the SAD pattern. However, for the medium fluence film, the amorphous surface layer is rippled and contains embedded GaAs crystallites. Correspondingly, for the medium fluence film, the SAD pattern contains both a diffuse halo and diffraction spots, indicative of the presence of crystallites within a-GaAs. To verify the presence and composition of these crystallites, the microstructure of the medium fluence film was further

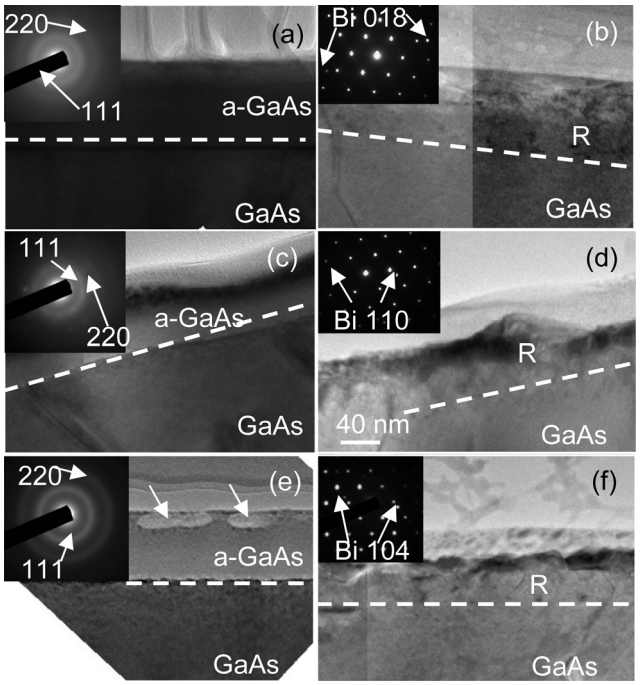

FIG. 1. Bright-field TEM images of (a), (b) low; (c), (d) medium; and (e), (f) high ion fluence films following implantation and implantation plus RTA, respectively. The insets in (a)–(f) are the corresponding SAD patterns. Following implantation, the BF-TEM images in (a), (c), and (e) reveal opaque regions at the surface, while the SAD patterns consist of diffuse halos, both indicating the formation of an amorphous surface layer. Following implantation plus RTA, the amorphous surface layer has recrystallized into single-crystal GaAs layers, denoted by the label "R" in (b), (d), and (f). The corresponding SAD patterns reveal diffraction spots, which are identified as the {018}, {110}, and {104} diffraction spots from bismuth. For the high ion fluence film in (e), >40 nm sized ovoid regions within the a-GaAs layer, labeled with arrows, are attributed to voids. In (f), ovoid regions are not apparent, suggesting that the voids collapsed during RTA.

examined using bright- and dark-field TEM. Close-up views of the as-implanted medium fluence GaAs:Bi film are shown in Fig. 2(a) bright-field and Fig. 2(b) dark-field images. The dark-field image in Fig. 2(b) was obtained using the GaAs {111} diffraction spot. Of particular interest is the 40 nm feature circled in Figs. 2(a) and 2(b). Since the feature appears bright in Fig. 2(b), it is attributed to a GaAs crystallite. For the high fluence film, >40 nm ovoid regions in the amorphous GaAs layer are attributed to voids.

We now consider the influence of annealing on the microstructure of the GaAs:Bi films. Figures 1(b), 1(d), and 1(f) present typical bright-field TEM images (with corresponding SAD patterns as insets) of the annealed low, medium, and high fluence films, respectively. Following RTA, a ~85 nm surface layer (labeled "R") is observed on top of single-crystal GaAs, independent of ion fluence. The SAD patterns inset into Figs. 1(b), 1(d), and 1(f) show diffraction spots with d-spacings of 3.25 Å, within <1% of the {111} interplanar spacing of GaAs, indicating that the surface layers are recrystallized GaAs. Interestingly, these SAD patterns also include diffraction spots with d-spacings of 1.38 Å (Fig. 1(b)), 2.26 Å (Fig. 1(d)), and 2.36 Å (Fig. 1(f)), within 1% of the {018}, {110}, and {104} interplanar spacing of Bi, respectively, implying the presence of Bi NCs embedded within single-crystal GaAs. We note that additional bright-field images spanning >0.08 μm^2 reveal Bi NCs with an average diameter of 34 ± 10 nm.

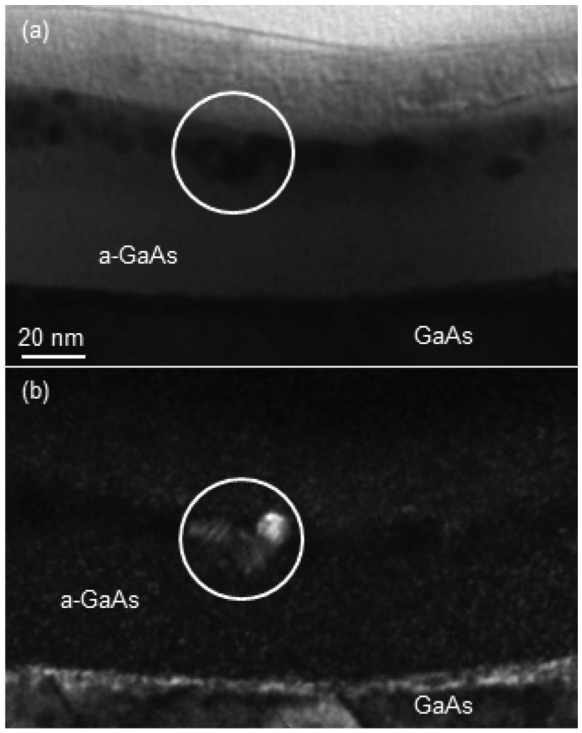

FIG. 2. TEM images of the medium fluence film following implantation: (a) transmitted beam bright-field and (b) dark-field using the GaAs {111} diffracted beam. The opaque feature apparent in the (a) bright-field image, which appears bright in the corresponding (b) dark-field image is attributed to a GaAs crystallite.

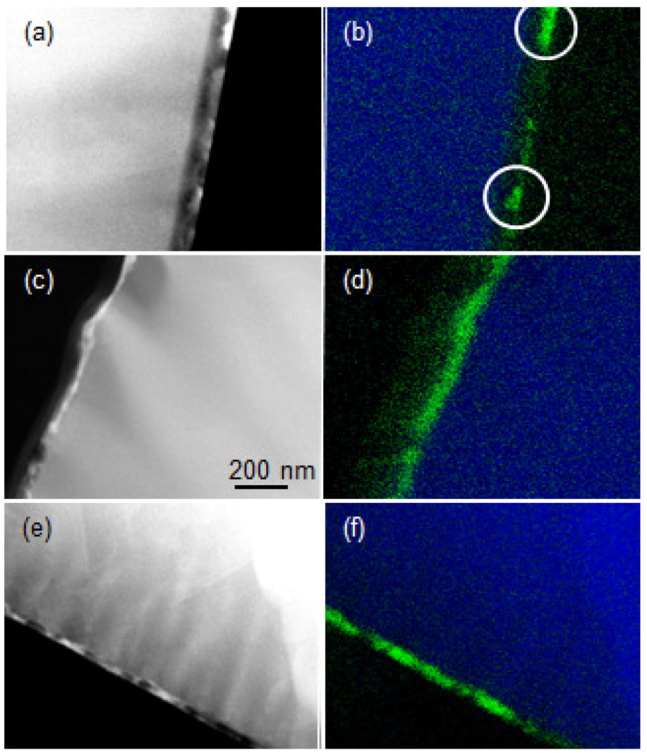

FIG. 3. Cross-sectional HAADF STEM images (a) low, (c) medium, and (e) high ion fluence GaAs:Bi films following RTA. The corresponding composite elemental maps of Ga (blue) and Bi (green) collected from (a), (c), and (e) are presented in (b), (d), and (f), respectively. The Bi NCs in (b) are circled as a guide to the eye, while a Bi-rich layer is observed in (d) and (f). All images share the scale used in (c).

To confirm the presence of Bi NCs in the GaAs:Bi films, HAADF imaging and EDX elemental mapping were conducted. Figure 3 presents typical HAADF images of post-RTA GaAs:Bi implanted at (a) low, (c) medium, and (e) high fluences. The corresponding EDX elemental maps are shown in Figs. 3(b), 3(d), and 3(f), with Bi and Ga atoms labeled in green and blue, respectively. EDX reveals the formation of approximately 80 to 150 nm Bi clusters (45–60 nm thick Bi-rich layers) for the low (medium and high) fluence film. The Bi clusters and Bi-rich regions are consistent with the Bi diffraction spots observed in Figs. 1(b), 1(d), and 1(f), indicating the presence of elemental Bi crystals.

It is interesting to note that these GaAs:Bi films were subjected to similar implantation fluences and annealing conditions as the poly-GaAs:In films discussed in Ref. 8. In the case of indium irradiation of GaAs, RTA at 450 °C led to the nucleation of In NCs within a polycrystalline GaAs matrix; hence, "poly-GaAs:In." However, for these GaAs:Bi films, RTA at 450 °C leads to Bi NC nucleation within a single-crystal GaAs matrix. This difference in recrystallization is presumably due to the catalytic effect of Bi on GaAs recrystallization. Interestingly, Bi has been shown to increase the surface diffusion length of Ga and As atoms during epitaxial growth of both stoichiometric and As-rich GaAs.[18] We hypothesize that the presence of Bi within the a-GaAs films enables the GaAs film to fully recrystallize.

B. Influence of Bi NCs on the Seebeck coefficient

To examine the influence of the Bi NCs on the Seebeck effect in GaAs:Bi, we consider the T-dependence of S of the implanted plus annealed films, in comparison with those of the GaAs reference, as shown in Fig. 4. At the lowest measurement temperatures, both the Bi NC-containing and reference GaAs films exhibit a rapid increase of $|S|$ up to a peak at ~10 K, similar to earlier reports of poly-GaAs:In.[15] In both cases, for $T > 10$ K, $|S|$ rapidly decreases with increasing temperature to ~100 K. This T-dependence of S is a manifestation of a strong electron-phonon interaction, referred to as the phonon-drag effect. For the low and

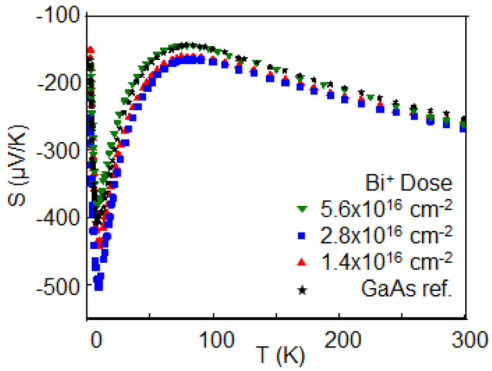

FIG. 4. Seebeck coefficient, S, as a function of temperature for the low, medium, and high fluence GaAs:Bi films following RTA, relative to that of the reference film. For $T < 100$ K, the maximum value of $|S|$ for both the low and medium fluence films is greater than that of the reference, while $|S|$ of the high fluence film is less than that of the reference. For $T > 100$ K, $|S|$ of the GaAs:Bi films and the GaAs reference are similar.

medium fluence GaAs:Bi films, the maximum values of $|S|$ are 10% and 25% higher than that of the GaAs reference, presumably due to free carrier trapping at implantation-induced defects. On the other hand, for the high fluence GaAs:Bi film, the maximum value of $|S|$ is reduced by 8% in comparison to that of the GaAs reference, presumably due to *enhanced* phonon scattering at vacancies.[19] Indeed, the absence of voids in the high fluence GaAs:Bi film following RTA suggests RTA-induced atomic diffusion into the voids, resulting in an increased concentration of vacancies. For $T > 100$ K, in the regime where electron diffusion is driven by the temperature gradient (the "diffusion" regime), $|S|$ increases monotonically with T, for all films, independent of implantation dose. Thus, Bi NCs have a negligible influence on $|S|$ of GaAs, similar to the negligible effect of In NCs or GaAs grain boundaries reported earlier.[8] Indeed, the S of the poly-GaAs:In and GaAs:Bi films is similar to those of bulk GaAs with a similar free carrier concentration.[20] Therefore, increases in $|S|$ are primarily due to the decreases in n, rather than any density of states modifications due to the presence of Bi or In NCs in single or polycrystalline GaAs.

C. Influence of microstructure on electrical properties

We now consider the influence of microstructure on the relationship between the free carrier concentration, n, and the electrical conductivity, σ, of the GaAs:Bi films in comparison with those of poly-GaAs:In[8] and GaAs:N,[21] as shown in Fig. 5(a). In the plot of σ vs. n, dashed lines form an "envelope" corresponding to a mobility range of 1000–4000 $cm^2\ V^{-1}s^{-1}$. It is interesting to note that all GaAs-based films lie within this envelope, independent of implantation fluence and species. The GaAs film mobilities are typically near the upper end of the range (4000 $cm^2\ V^{-1}s^{-1}$), while the GaAs:Bi, poly-GaAs:In, and GaAs:N mobilities range from near the lower end (1000 $cm^2\ V^{-1}s^{-1}$) to the mid-range of the envelope, depending on their microstructure. For example, the mobilities of the as-implanted GaAs:Bi, poly-GaAs:In, and GaAs:N films, which consist of amorphous layers, lie near the lower end of the range. Similarly, the mobility of the poly-GaAs:In film following RTA, with a polycrystalline microstructure, lies near the lower end of this range. Meanwhile, the mobilities of the recrystallized GaAs:Bi films (following RTA), lie near the mid-range of the envelope. The trends for n are similar. Following implantation with Bi, In, or N, n is reduced in comparison to that of the GaAs reference films, presumably due to an increase in the concentration of implantation-induced point defects which trap carriers.[22] It is interesting to note that n of the as-implanted GaAs:Bi film with crystalline remnants is higher than those as-implanted GaAs:Bi films without crystalline remnants, consistent with the increase in active dopant concentration expected in crystalline versus amorphous GaAs.[23] Following RTA, both n and σ of the implanted GaAs films increase, most likely due to the annealing out of defects that trap carriers. It is interesting to note that n is doubled in the presence of In NCs. Since the work function of In (defined as the difference between the vacuum level and the Fermi Energy) and the electron affinity of GaAs (defined as the difference between the vacuum level and the conduction band edge) differ by 0.05 eV,[24] it is likely that the In NCs act as electron donors, similar to reports of ErAs particles embedded in GaAs.[25] However, since the difference between the work function of Bi and the electron affinity of GaAs is 0.15 eV below the GaAs conduction band edge,[24] the Bi NCs are not expected to act as electron donors.

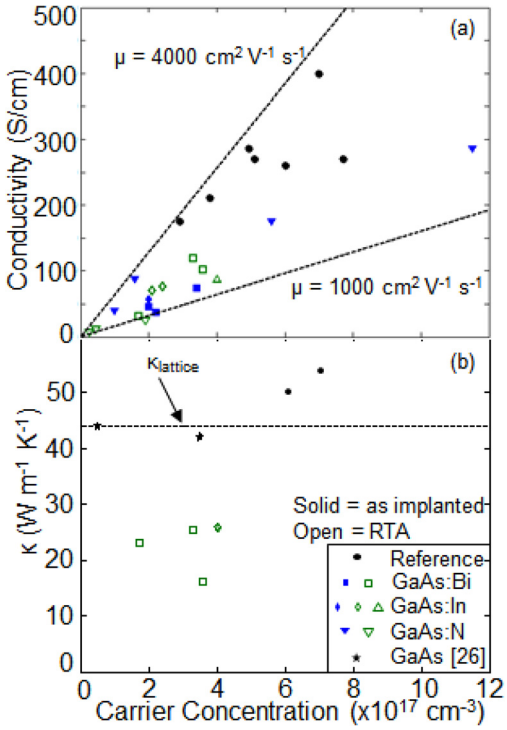

FIG. 5. (a) Electrical conductivity, σ, and (b) thermal conductivity, κ, as a function of free carrier concentration, n. The black points correspond to GaAs reference films, while the solid blue and open green points correspond to GaAs:Bi films following implantation and implantation plus RTA, respectively. For the poly-GaAs:In, the open diamonds correspond to the lowest RTA temperature, while the upward triangle represents the medium and high RTA temperatures. For all films, the mobility falls within an "envelope" ranging from 1000–4000 $cm^2\ V^{-1}s^{-1}$. For all implanted-plus-annealed films, the thermal conductivities are significantly lower than those of the GaAs reference, presumably due to phonon scattering at NC boundaries.

D. Influence of microstructure on thermal properties

We consider the role of microstructure on κ as a function of free carrier concentration, n, for the GaAs:Bi films in comparison with those of poly-GaAs:In[8] and bulk GaAs,[26] as shown in Fig. 5(b). For GaAs, since κ is weakly dependent on n, the electronic contribution to κ is negligible; thus, we consider $\kappa_{total} \approx \kappa_{lattice}$,[26] shown as the nearly horizontal dashed line in the plot in Fig. 5(b). For the GaAs reference, $\kappa \approx 50$ W $m^{-1}K^{-1}$; on the other hand, both poly-GaAs:In and GaAs:Bi exhibit a significantly reduced κ in comparison to that of the GaAs reference films. Following the Bi implantation plus annealing, κ is reduced to 16–26 W $m^{-1}K^{-1}$, which corresponds to 30%–50% of the κ of the GaAs reference, presumably due to phonon scattering at NC boundaries.

To determine the effect of Bi implantation-plus-annealing on the thermoelectric properties of GaAs, we now consider ZT in comparison to that of the GaAs reference films. Considering the reduced electrical conductivity and Seebeck coefficient induced by Bi implantation plus annealing, the reductions in κ lead to a ~30% improvement in the room temperature figure-of-merit, Z. For further reductions in κ without compromising σ or $|S|$ values, it will be important to tailor the nanoinclusion density and size.

IV. SUMMARY AND CONCLUSIONS

In summary, we examined the formation of embedded Bi NCs and their influence on the thermoelectric properties of GaAs, observing a ~30% increase in the room temperature Z. Bi implantation leads to the formation of a-GaAs with or without crystalline remnants, voids, and/or ripples. Implantation-induced defects trap carriers, reducing both n and σ. Following RTA, the matrix transforms to single crystal GaAs with embedded Bi NCs, while a partial recovery of n and σ is observed. The presence of Bi NCs leads to a reduction in κ to 30%–50% of the GaAs reference value, presumably due to nanostructuring within a reduced-κ matrix. A comparison of GaAs:Bi, poly-GaAs:In, and GaAs:N films reveals a universal trend for the influence of microstructure on the n-dependence of σ and κ.

ACKNOWLEDGMENTS

This research was supported by the Center for Solar and Thermal Energy Conversion, an Energy Frontier Research Center funded by the U.S. Department of Energy, Office of Science, Office of Basic Energy Science under Award No. DE-SC0000957.

APPENDIX: ANALYSIS OF TIME-DOMAIN THERMOREFLECTANCE DATA

The TDTR data were analyzed, as follows. Figure 6 shows the time-dependence of the normalized reflectance for both the Bi NC-containing films and a GaAs reference film,

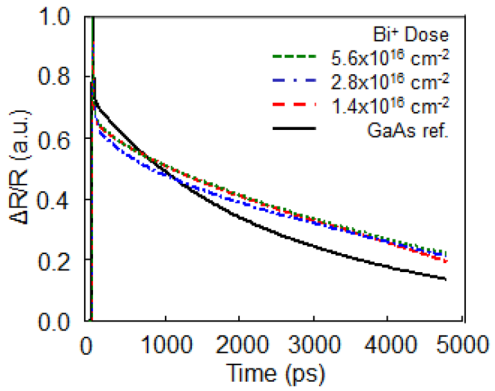

FIG. 6. Normalized transient thermoreflectance as a function of time for the low, medium, and high fluence GaAs:Bi films, in comparison to that of the GaAs reference. Since the reflectance decay time is longer for the GaAs:Bi films than for the GaAs reference, the surface of GaAs:Bi cools more slowly than the surface of the GaAs reference. This data suggests a reduced thermal conductivity for GaAs:Bi relative to that of the GaAs reference.

with $t = 0$ corresponding to the initiation of the pump pulse. During the first 100 ps, the metallic transducer is heated, leading to a rise in reflectance. From 200 to 4700 ps following the pump pulse, heat is dissipated through the Bi NC-containing (GaAs) layer in the nanocomposite (reference) films, leading to a gradual decrease in thermoreflectance. To extract the thermal conductivity of the GaAs:Bi and GaAs reference films, the decay time associated with heat flow away from the films is determined using the one-dimensional diffusion equation,[27] with the energy flux into the film set equal to the energy flux lost from the transducer (which is assumed to have the same κ as bulk Al, i.e., $\kappa_{transducer} = \kappa_{Al} = 200\,W\ m^{-1}\ K^{-1}$).[28] Using the thermal boundary conductance reported for Al/GaSb[29] as the upper bound for our Al/GaAs reference films, we use a least-squares minimization algorithm to solve for the thermal boundary conductance of the Al/GaAs:Bi films, κ_{film}.

[1]L. D. Hicks, T. C. Harman, X. Sun, and M. S. Dresselhaus, Phys. Rev. B **53**, R10493 (1996).
[2]R. Venkatasubramanian, E. Siivola, T. Colpitts, and B. O'Quinn, Nature **413**, 597 (2001).
[3]M. Zebarjadi, G. Joshi, G. Zhu, B. Yu, A. Minnich, Y. Lan, X. Wang, M. Dresselhaus, Z. Ren, and G. Chen, Nano Lett. **11**, 2225 (2011).
[4]D.-K. Ko, Y. Kang, and C. B. Murray, Nano Lett. **11**, 2841 (2011).
[5]F. Hao, D. Fang, and Z. Xu, Appl. Phys. Lett. **100**, 091903 (2012).
[6]L. Bertini, K. Biliquist, M. Christensen, C. Gatti, L. Holmgren, B. Iversen, E. Mueller, M. Muhammed, G. Noriega, A. Palmqvist, D. Platzek, D. M. Rowe, A. Saramat, C. Stiewe, M. Toprak, S. G. Williams, and Y. Zhang, in *22nd International Conference on Thermoelectrics, ICT* (2003), p. 93.
[7]A. G. Every, Y. Tzou, D. P. H. Hasselman, and R. Raj, Acta Metall. Mater. **40**, 123 (1992).
[8]M. V. Warren, J. C. Canniff, H. Chi, E. Morag, F. Naab, V. A. Stoica, R. Clarke, C. Uher, and R. S. Goldman, J. Appl. Phys. **114**, 043704 (2013).
[9]S. B. Evgenev and N. V. Ganina, Izv. Akad. Nauk SSSR, Neorg. Mater. **20**, 561 (1982) [Inorganic Materials 20, 479 (1984)].
[10]F. Komarov, L. Vlasukova, V. Yuvchenko, T. Petlitzkaya, and P. Zukowski, Vacuum **78**, 353 (2005).
[11]J. L. Merz, L. C. Feldman, and E. A. Sadowski, Radiat. Eff. **6**, 285 (1970).
[12]M. J. Seong and A. Mascarenhas, private communication (July 23, 2013).
[13]B. Lita, S. Ghaisas, R. S. Goldman, and M. R. Melloch, Appl. Phys. Lett. **75**, 4082 (1999).
[14]N. Mingo, Appl. Phys. Lett. **84**, 2652 (2004).
[15]M. V. Warren, A. W. Wood, J. C. Canniff, F. Naab, C. Uher, and R. S. Goldman, Appl. Phys. Lett. **100**, 102101 (2012).
[16]W. Kim, J. Zide, A. Gossard, D. Klenov, S. Stemmer, A. Shakouri, and A. Majumdar, Phys. Rev. Lett. **96**, 045901 (2006).
[17]V. A. Stoica, Y.-M. Sheu, D. A. Reis, and R. Clarke, Opt Express **16**, 2322 (2008).
[18]S. Tixier, M. Adamcyk, E. C. Young, J. H. Schmid, and T. Tiedje, J. Cryst. Growth **251**, 449 (2003).
[19]G. J. Snyder and E. S. Toberer, Nat. Mater. **7**, 105 (2008).
[20]S. K. Sutradhar and D. Chattopadhyay, J. Phys. C: Solid State Phys. **12**, 1693 (1979).
[21]R. R. Collino, "Blister formation and layer transfer of N-implanted GaAs," Ph.D. thesis (University of Michigan, 2010).
[22]R. Coates and E. W. Mitchell, J. Phys. C: Solid State Phys. **5**, L113 (1972).
[23]W. G. Opyd, J. F. Gibbons, and A. J. Mardinly, Appl. Phys. Lett. **53**, 1515 (1988).
[24]H. B. Michaelson, J. Appl. Phys. **48**, 4729 (1977).
[25]J. M. Zide, D. O. Klenov, S. Stemmer, A. C. Gossard, G. Zeng, J. E. Bowers, D. Vashaee, and A. Shakouri, Appl. Phys. Lett. **87**, 112102 (2005).
[26]A. Amith, I. Kudman, and E. F. Steigmeier, Phys. Rev. **138**, A1270 (1965).
[27]R. J. Stevens, A. N. Smith, and P. M. Norris, J. Heat Transfer **127**, 315 (2005).
[28]F. Cverna, *ASM Ready Reference: Thermal Properties of Metals* (ASM International, 2002).
[29]P. E. Hopkins, J. C. Duda, S. P. Clark, C. P. Hains, T. J. Rotter, L. M. Phinney, and G. Balakrishnan, Appl. Phys. Lett. **98**, 161913 (2011).